Forest Ecology and Management 294 (2013) 136–149

Contents lists available at SciVerse ScienceDirect

Forest Ecology and Management

journal homepage: www.elsevier.com/locate/foreco

Real time simulation of 2007 Santa Ana fires

A.K. Kochanski [a,*], M.A. Jenkins [b], J. Mandel [c], J.D. Beezley [d], S.K. Krueger [a]

[a] Department of Atmospheric Sciences, University of Utah, Salt Lake City, UT, United States
[b] Department of Earth and Space Science and Engineering, Lassonde School of Engineering, Toronto, Ontario, Canada
[c] Department of Mathematical and Statistical Sciences, University of Colorado, Denver, United States
[d] Météo France and CERFACS, Toulouse, France

ARTICLE INFO

Article history:
Available online 18 January 2013

Keywords:
Wildfire
Modeling
Fire
Forecasting
Fire spread prediction
Santa Ana

ABSTRACT

In this study we test the feasibility of using a coupled atmosphere–fire model for real time simulations of massive fires. A physics-based coupled atmosphere–fire model is used to resolve the large-scale and local weather as well as the atmosphere–fire interactions, while combustion is represented simply using an existing operational surface fire behavior model. This model combination strikes a balance between fidelity and speed of execution. The feasibility of this approach is examined based on an analysis of a numerical simulation of two very large Santa Ana fires using WRF–Sfire, a coupled atmosphere–fire model developed by the Open Wild Fire Modeling Community (OpenWFM.org). The study demonstrates that a wind and fire spread forecast of reasonable accuracy was obtained at an execution speed that would have made real-time wildfire forecasting of this event possible.

1. Introduction

There are multiple simulator models for operational forecasting of forest fire propagation as shown by Papadopoulos and Pavlidou (2011), and Sullivan (2009), who examine each simulator in turn, discussing their attributes and capabilities, along with their drawbacks and deficiencies. The conclusion of both studies is that, of the existing simulators, FARSITE is the most precise. To ensure the best forecast, FARSITE necessitates ingestion of multiple layers of data. Spatially-gridded GIS observational data on fuels and topography are required, and weather data are required to provide surface wind speed and direction, temperature, humidity, and cloud cover at time of ignition. The primary end product of FARSITE is the prediction of a fire perimeter over the fire's landscape. Sullivan (2009) points out that current operational fire-spread models are a conversion of one-dimensional linear models of fire spread to two-dimensional models of fire spread, and FARSITE is no exception. FARSITE is based on BEHAVE (Andrews, 1986) which is based on the rate-of-spread (ROS) model by Rothermel (1972).

Despite its wide spread use in the United States and elsewhere, FARSITE, along with the other operational fire-spread formulations discussed by Papadopoulos and Pavlidou (2011), and Sullivan (2009), suffer from one fundamental defect, and that is their simplistic treatment of the wind on fire behavior. These models consider only surface wind direction and strength, they lack a real-time wind and weather forecast component, and they fail to account for coupled atmosphere/wildfire interactions.

In the scientific community there exist a significant number of physics-based fluid-dynamical deterministic numerical modeling studies (e.g., Mell et al., 2007; Colman and Linn, 2007; Coen, 2005; Sun et al., 2009; Mandel et al., 2011) demonstrating the significant impacts changing environmental wind conditions and coupled atmosphere/fire flow have on wildland fire propagation. Despite the physical validity of a fluid-dynamical coupled atmosphere/fire numerical model for predicting fire spread, operational application of this type of model is thought to be beyond present computing capabilities. The prevailing view in both scientific and operational communities is that wildfire behavior prediction using this modeling approach must therefore remain relegated to the study of wildfires under conditions not amenable to field experimentation.

The physics-based models like FIRETEC (Colman and Linn, 2007) and WFDS (Mell et al., 2007) attempt to resolve the combustion-related processes without parameterizing the fire spread. Because of this, these models require very high resolution, which in turn limits the maximum size of the model domain and the simulated fire. Therefore, all previous attempts at coupled atmosphere–fire numerical simulations of actual fires have been performed at very high resolutions for relatively small fires. The numerical study of the Calabasas fire by Bossert et al. (2000) utilized the fully-coupled HIGRAD/FIRETEC, model run at 10 m horizontal resolution, for an area of 1.27 km × 1.27 km. Even higher spatial resolution and consequently also smaller domain were used by Linn et al. (2010), where the same model was run at 2 m horizontal resolution for a single 900 m × 900 m domain. Also the simulations of the Big Elk fire by Coen (2005), using Clark et al. (2004) coupled atmosphere–fire model at a very high resolution (41 m) from a forecast-

* Corresponding author.
E-mail address: adam.kochanski@utah.edu (A.K. Kochanski).

0378-1127/$ - see front matter © 2012 Elsevier B.V. All rights reserved.
http://dx.doi.org/10.1016/j.foreco.2012.12.014

ing point of view, covered a relatively small area of roughly 5.3 km × 5.3 km. Of these studies, only Coen (2005), using a parameterized fire spread, came close to a real-time forecast using readily available computing resources.

Another attempt to include changing environmental wind conditions, but no coupled atmosphere/fire flow, was presented by Weise et al. (2007). They utilized the FARSITE fire model with winds supplied by MM5 (http://www.mmm.ucar.edu/mm5/), a regional spectral weather forecast model, run at horizontal resolutions of 5 km and 1 km, respectively. A simulation of the 2006 Esperanza fire was used to demonstrate the operational utility of their approach, which burnt an area 161.37 km^2, an order of magnitude greater than the combined areas of the numerical experiments mentioned above.

In this study we have chosen to use the WRF–Sfire, a physically-based coupled atmosphere–fire modeling system that parameterizes fire spread, to simulate two wildland fires that ignited, burned, and merged, during a 2007 Santa Ana weather event. Our overall objective is to test the feasibility of WRF–Sfire for accurate real-time forecasting of wildfire behavior. To achieve this objective, we perform, using readily available computing capabilities, along with spatially-gridded GIS data on fuels and topography, a faster-than-real-time simulation of these two 2007 Santa Ana fires, and compare the results to available weather and fire observations.

We analyze the WRF–Sfire numerical simulation of Witch and Guejito fires which started on 21 October 2007 at 12:15 pm local time (19:15 UTC) and 22 October 2007 at 01:00 am local time (08:00 UTC), respectively. They spread under strong Santa Ana winds, eventually burning 80,156 ha (801.56 km^2), and leading to $18 millions in damage and two fatalities. Together they were the second largest fire event of the 2007 California wildfire season (Keeley et al., 2009).

The paper is organized as follows. We describe the WRF–Sfire and its forecasting abilities in Section 2. In Section 3 we present a WRF–Sfire model setup that allows for real-time weather and fire-spread prediction. Using this model configuration and setting the initial fuel and weather conditions based on data described in Section 3.2, the WRF–Sfire was run for each fire and final wildfire forecasts were produced. The accuracy of the model results are analyzed: first in terms of providing a realistic wind forecast, and second in terms of providing a realistic fire-spread forecast. These results are presented, respectively, in Sections 4.1 and 4.2, where we compare simulated to observed winds in the vicinity of the fires, and simulated to observed fire progression and final fire perimeters. The paper is summarized and conclusions are given in Section 5.

2. Model description

WRF–Sfire is a coupled atmosphere–fire model, developed by the Open Wild Fire Modeling Community (OpenWFM.org). It combines the WRF (Weather Research and Forecasting system) (Skamarock et al., 2008) with fire propagation (Patton and Coen, 2004) calculated by the level set method (Mandel et al., 2009). The two-dimensional surface propagation of the fire perimeter is modeled by the advection of the level set function by the local fire ROS. WRF–Sfire can be categorized as a quasi-physical model since it includes the physics of the coupled fire/atmosphere, but does not attempt to represent the chemistry of fire spread. Instead the ROS is computed based on local fuel properties, slope, and wind speed using the semi-empirical Rothermel fire spread model (Rothermel, 1972). In this way, the computational costs of the WRF–Sfire remain reasonable while, unlike existing operational fire spread models, atmosphere/fire coupled WRF–Sfire winds at the fire line are used to compute the surface fire spread, amount of fuel burned, and propagation of the fire front. Coupling between the fire and the atmosphere occurs mainly through the release of latent and sensible heat at the surface by the fire into the WRF model atmosphere. The rate and amount of latent and sensible heat released depend on the fire perimeter's ROS as it evolves in time. As a result the model atmosphere "feels the fire" and responds to it by changing air temperature, density, humidity, pressure, and the local wind field. This coupled fire/atmosphere local wind affects the fire spread and its intensity, allowing for a constant feedback between the fire and atmosphere. Fig. 1 illustrates the two-way fire–atmosphere coupling used in WRF–Sfire.

The incorporation of WRF–Sfire into the WRF modeling framework (which is used for routine numerical weather prediction in the United States) allows for detailed descriptions of the land use, fuel types, and topography (Beezley, 2011a, 2011b), and for realistic setup of fire–atmosphere simulations affected by terrain and time-varying larger-scale meteorological forcing. The nesting capabilities of WRF–Sfire (Fig. 2) allow for multi-scale simulations in which a coarse tens-of-kilometers resolution outer domain captures the large synoptic-scale flow and feeds a set of nested higher-resolution domains. In this way, larger-to-smaller scale flows are gradually resolved to finally represent coupled atmosphere/fire flows at the smallest resolved scale. In addition, complex terrain that can influence both large- and small-scale flow is rendered more accurately. To accommodate high-resolution fuel and elevation data, and to provide sufficient accuracy for the fire spread computation without increasing computational cost, the fire model operates on a separate surface model grid refined significantly with respect to the atmospheric model (usually 15–25 times denser). Fire spread is therefore forecast at a resolution much finer than the resolution of the weather component of the WRF model. An example of the nested setup used for this study is presented in Fig. 1. The nested setup and vertical-grid refinement provide localized fire spread and weather predictions at significantly higher resolutions than currently available from NOAA (i.e., hundreds of meters resolution versus 12 km resolution). To date the WRF–Sfire was tested on prescribed FireFlux fire (Kochanski et al., 2010), Meadow Creek fire in Colorado (Beezley et al., 2010), Bulgaria fires (Dobrinkova et al., 2011; Jordanov et al., 2011) and 2007 Kangaroo Island bushfires (Mika Peace et al., 2011), that occurred in grass, forest, mixed (grass, brush, forest), and shrub fuels.

3. Experimental setup

3.1. Model configuration

The Witch and Guejito fires simulated in this study were driven by strong westerly Santa Ana winds induced by a high-pressure system located over northern Nevada. As the pressure built up and the system moved eastward, southern California began to experience very strong and gusty Santa Ana winds that brought very warm and dry air from the Nevada desert into the San Diego area (Schroeder, 1964; Fosberg et al., 1966). In order to resolve the development and movement of this large-scale weather system, together with the local circulation that is affected strongly by the complex topography of southern California, WRF was configured with four nested domains: D01, D02, D03, and D04, of horizontal-grid sizes 32 km, 8 km, 2 km, and 500 m, respectively. The domain setup used in this study is shown in Fig. 2. A vertically-stretched grid was used to provide high vertical resolution at the surface ($\Delta Z \sim 20$ m), decreasing to coarser resolution ($\Delta Z \sim 500$ m) between 3.5 and 7.5 km altitude, and decreasing further ($\Delta Z \sim 2000$ m) at the model top at 15.4 km altitude. The fire domain was embedded within the domain (D04) of finest (500 m)

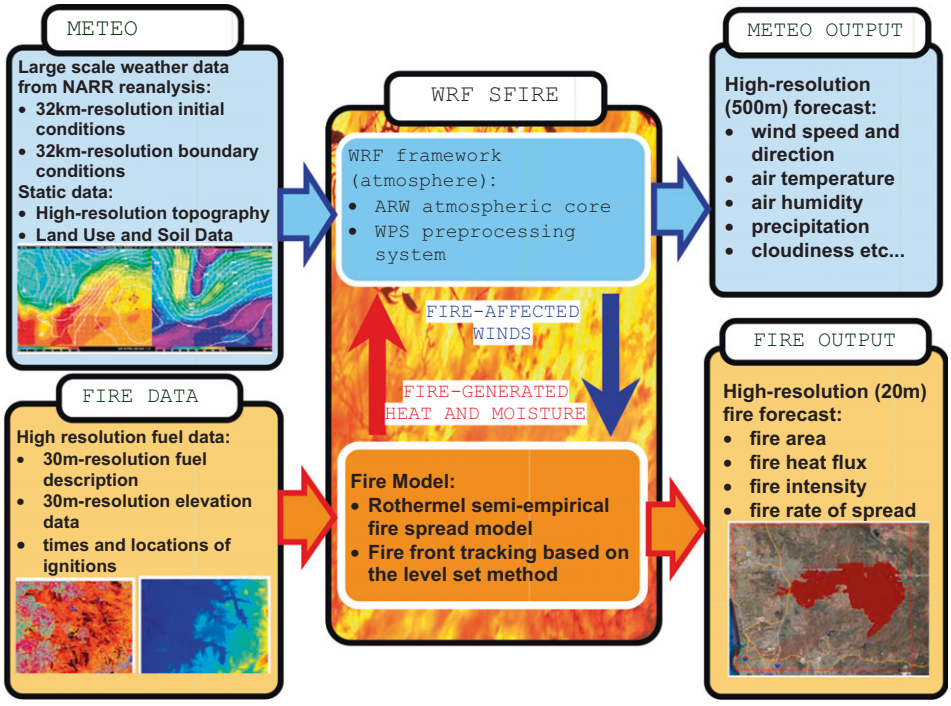

Fig. 1. Diagram of the WRF–Sfire coupled fire–atmosphere modeling system. ARW stands for Weather Research & Forecasting – Advanced Research WRF.

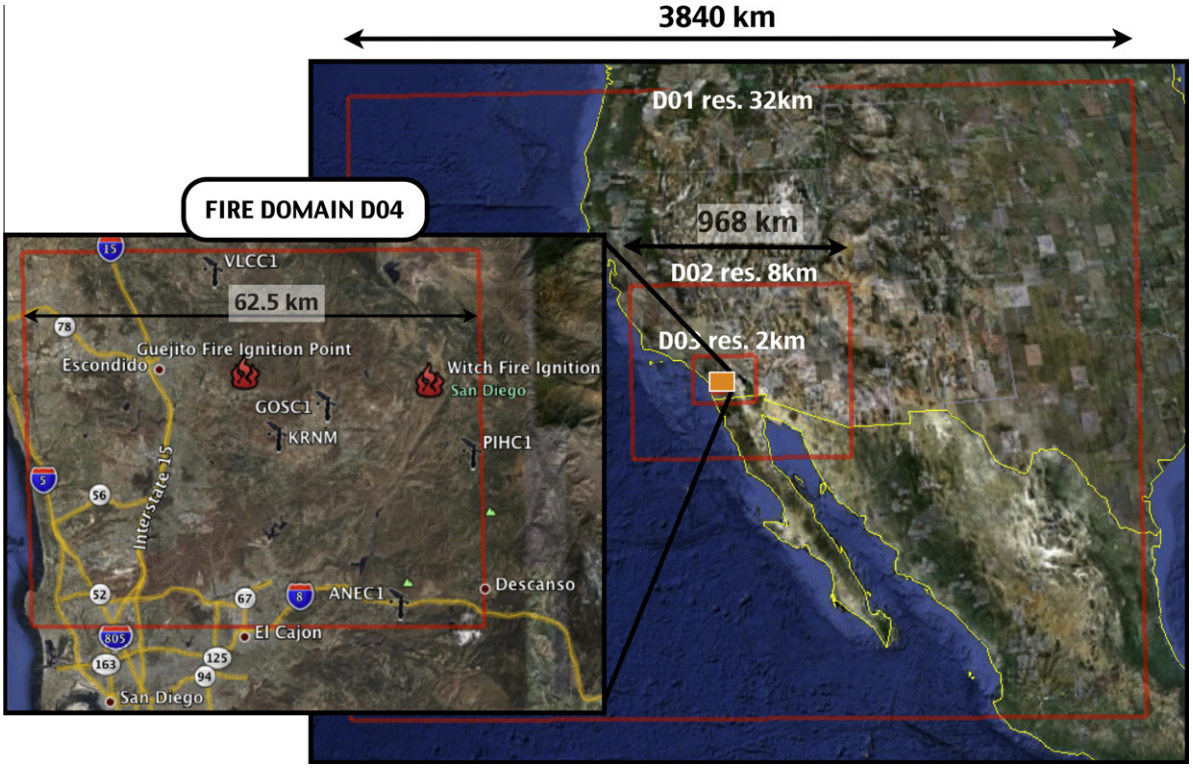

Fig. 2. The multi-scale WRF setup in this study, with locations of fire origins and local meteorological stations used for model validation. Horizontal domain resolutions vary from 32 km (D01) to 500 m (D04).

resolution. The WRF–Sfire atmosphere–fire refinement ratio in the X (east–west) and Y (north–south) directions was set at 25, making the horizontal fire-grid length 20 m. The details of the model configuration are presented in Table 1.

The 72 h forecast presented in this study was run on 10 dual Intel Xeon X5670 nodes connected using QDR Infiniband links. Each node was equipped with two 6-core CPUs, so there were 12-cores available for each node. The entire 72 h forecast was computed in

Table 1
Details of the WRF–Sfire setup.

Domain	Atmospheric domain size $X \times Y \times Z$	Atmospheric horizontal resolution $\Delta X \times \Delta Y$	Atmospheric vertical grid resolution ΔZ (m)	Fire domain size $X_f \times Y_f$	Fire domain resolution $\Delta X_f \times \Delta Y_f$
D01	120 × 96 × 37	32 km × 32 km	20–2000	–	–
D02	121 × 97 × 37	8 km × 8 km	20–2000	–	–
D03	137 × 105 × 37	2 km × 2 km	20–2000	–	–
D04	125 × 105 × 37	500 m × 500 m	20–2000	3125 × 2625	20 m × 20 m

4 h 48 min, while the first 24 h was ready in 1 h 35 min. The model output was saved at 10 min intervals.

3.2. Data sources

The atmospheric component of the WRF–Sfire was initialized with the North American Regional Reanalysis (NARR) dataset. NARR surface and upper-air meteorological observations of wind, temperature, humidity, and pressure provided the 3D description of the initial WRF–Sfire atmospheric state. The same dataset was also used to create boundary conditions for the outer-most domain. The three outer domains of the atmospheric component of WRF–Sfire (i.e., D01, D02, and D03) used MODIS-derived land-use categories and topography, while the innermost domain (D04) that contained the fire used 30 m resolution National Elevation Dataset (NED) obtained from the USGS Seamless Data Warehouse (http://seamless.usgs.gov/) interpolated to 500 m.

The fire model was initialized with 30 m resolution fuel data from LANDFIRE (Ryan et al., 2006; Rollins, 2009) in the form of 13 fuel categories as defined by Albini (1976). The special LANDFIRE categories not supported by the Rothermel model, like urban (91), snow/ice (92), and agriculture (93), were treated as missing data. The pixels marked as missing data were replaced with the prevailing categories of their surroundings using the nearest-neighbor average option available in the WRF preprocessing system (WPS). Water (98) and barren lands (99) were converted into the no-fuel category (14). Even though the resolution of the fire data is very high, an analysis of the fuel maps revealed that some of the rivers (for example the San Diego River) were not represented as continuous contours. Therefore the fuel map was compared with the visible satellite image from Google Earth and the discontinuities were fixed manually. Additionally, the residential area of Ramona, represented in the fuel data as brush categories (5 and 6), was contoured as a no-fuel category to prevent fire from penetrating into the urban area. The unintended impact of this was to represent to some degree the fire suppression activities that were employed there. The final processed fuel map used for the fire simulation is presented in Fig. 3. The topography for the fire model was obtained from the National Elevation Dataset (NED).

The model was modified to incorporate spatially variable fuel moisture, and initial fuel moisture was determined at the moment of the ignition of the Guejito fire. The fuel moisture map, presented in Fig. 4, is a composite of 1 h, 10 h and 100 h dead fuel moisture, as well as live fuel moisture using relative fuel loads derived from Albini (1976). The 1 h dead fuel moisture was estimated based on the simulated air temperature and relative humidity following Van Wagner and Pickett (1985). The 10 h dead fuel map was obtained by objective interpolation of the moisture data from six surface stations also presented in Fig. 4. The 100 h fuel moisture was set according to the estimates from the National Fuel Moisture Database distributed through the Wildland Fire Assessment System and available at http://www.wfas.net. The live fuel moisture was computed as an average of chamise chaparral moisture recorded at 4S Ranch and El Apajo fuel moisture stations (see Fig. 4).

4. Model results and validation

In coupled atmosphere–fire simulations the predicted fire behavior depends on the accuracies of both the meteorological and the fire components of the model. An unrealistic wind forecast can quickly lead to erroneous fire spread estimates even if the fire model itself provides a perfect forecast of the fire spread. Likewise a perfect weather forecast can lead to erroneous fire spread prediction due to the inaccuracies of the fire model or the fuel data. The biases of these two models may combine leading to drastically unrealistic results when, for example, both wind and ROS as a function of wind are overestimated. The biases may also combine to compensate when, for example, the fire model overestimates the rate of spread but the atmospheric model underestimates the wind speed. In this study this problem is approached by separate analyses of the weather and fire forecasts as described in following sections.

4.1. Meteorological forecast

The wind field that controls fire propagation speed and direction is the three-dimensional time-varying coupled atmosphere–fire wind field, and wind is the primary meteorological factor affecting fire spread as simulated by WRF–Sfire. An evaluation of the fire spread forecast by WRF–Sfire starts therefore with an evaluation of the wind forecast by WRF.

There were 15 automated meteorological stations located within D04, the fire model domain. Unfortunately, because of very strong Santa Ana winds and the fire, the operations in many stations were disrupted. Due to missing data and data quality problems, eight stations were dropped from the analysis. From the seven remaining stations, four were selected, two in the center of the domain (GOSC1 and KRNM), one at the eastern boundary (PIHC1), and one at the northern model boundary (VLCC1), for analysis. The locations of these stations as well as origins of the Witch and Guejito fires are presented in Fig. 2.

The resolution of the WRF simulation affects to what degree the model resolves local topography. The elevation data as incorporated into WRF are an approximation of the real topography. The actual elevation of the meteorological reporting stations and the elevation of the model terrain at these locations differ generally by up 20 m. This bias in the WRF elevation must be considered when converting the model 10 m wind values to the 6.1 m height used for wind measurements at meteorological reporting stations. The simple power law formula by Sedepian (1980) is applied:

$$\mathrm{WS}_{6.1\ \mathrm{m}} = \mathrm{WS}_{10\ \mathrm{m}} \times \left(\frac{6.1}{10 + (\mathrm{HGT}_{\mathrm{WRF}} - \mathrm{HGT}_{\mathrm{ST}})} \right)^{\frac{1}{7}}, \quad (1)$$

where $\mathrm{WS}_{6.1\ \mathrm{m}}$ is the WRF-simulated wind speed adjusted to 6.1 m, $\mathrm{WS}_{10\ \mathrm{m}}$ is the 10 m wind speed from model output, $\mathrm{HGT}_{\mathrm{WRF}}$ is the elevation of station location on the model grid, and $\mathrm{HGT}_{\mathrm{ST}}$ is the true elevation of the meteorological station. Eq. (1) accounts for the total height bias between the model and the station due to the elevation mismatch ($\mathrm{HGT}_{\mathrm{WRF}} - \mathrm{HGT}_{\mathrm{ST}}$), and the difference between the sta-

tion reporting height (6.1 m) and the model wind output height (10 m).

The WRF–Sfire simulation started on October 21 at 5:00 am local time (12:00 UTC) and was run for the period of 72 h without updating the model state with current meteorological observations during the run. This means that, unlike an actual operational forecast during which the WRF state is automatically updated as the most current meteorological observations are assimilated, we did not interfere with the model as it ran. We provided the model with boundary conditions only at the initial stage and the WRF–Sfire model was not nudged towards the current observed state.

WRF–Sfire wind speeds and directions were interpolated linearly to the times when observational data were available and the following standard statistics were computed for the wind speed:

→ ME = mean of the difference between the simulated and observed data.
→ MAE = mean of the absolute value of the difference.
→ RMS = the root mean squared of the difference.
→ R = the sample correlation coefficient between the simulated and observed data.

Circular statistics following Jammalamadaka and Lund (2006) were used to determine wind directions. Circular statistics operate on the sines and the cosines of the wind directions, instead of the directions themselves, and the approach therefore avoids periodicity issues and preferred directions. First, the cosines and sines of the wind directions, instead of the directions themselves, from the simulation are interpolated to the data points. With c_i and s_i denoting these interpolated values, the angles at the interpolation points are then determined from the Cartesian to polar coordinate conversion:

$$\cos\theta_i = \frac{c_i}{\sqrt{c_i^2 + s_i^2}}, \quad \sin\theta_i = \frac{s_i}{\sqrt{c_i^2 + s_i^2}}. \tag{2}$$

Circular statistics are computed from the differences between simulated and observed sines and cosines. When the differences are small, this approach results in asymptotically the same results as using the directions themselves (i.e., $\sin\alpha \approx \alpha$ for small α in radians), but avoids non-uniqueness of directions (adding or subtracting 2π radians = 360° results in no change in the wind direction). Using φ_i, the wind directions from the data, the circular mean error, mean absolute error, and root of mean squares error (in degrees) are computed as

$$ME_C = \frac{180}{\pi}\frac{1}{n}\sum_{i=1}^{n}\sin(\theta_i - \varphi_i)$$

$$MAE_C = \frac{180}{\pi}\frac{1}{n}\sum_{i=1}^{n}|\sin(\theta_i - \varphi_i)|$$

$$RMSE_C = \frac{180}{\pi}\sqrt{\sum_{i=1}^{n}\frac{1}{n}\sin^2(\theta_i - \varphi_i)}$$

respectively.

Two circular correlation coefficients were computed. First, following Jammalamadaka and SenGupta (2001), the mean direction $\overline{\theta}$ is computed by taking the means of $\cos\theta_i$ and $\sin\theta_i$ and converting to polar coordinates as in (1). The mean data direction $\overline{\varphi}$ is calculated similarly. The circular correlation coefficient R_C is then computed as the sample correlation of the values $\sin(\theta_i - \overline{\theta})$ and $\sin(\varphi_i - \overline{\varphi})$. Second, the circular correlation coefficient of Fisher and Lee (1983) is computed using

$$R_T = \frac{\sum_{i,j}\sin(\theta_i - \theta_j)\sin(\varphi_i - \varphi_j)}{\sqrt{\sum_{i,j}\sin^2(\theta_i - \theta_j)}\sqrt{\sum_{i,j}\sin^2(\varphi_i - \varphi_j)}}.$$

These two correlation coefficients yield similar, though not identical values. The statistical analysis of the model results for the wind speed and direction are presented in Tables 2 and 3.

The time series of the forecasted and observed wind speeds, and wind directions at the four meteorological stations are presented in Fig. 5. According to meteorological convention, the wind direction is the direction the wind is blowing from, represented as an angle from the north: 0° means wind blowing from the north; 90° means from the east; 180° means from the south; and 270° means from the west. Fig. 5 shows the initially weak to moderate wind increasing very quickly as the Santa Ana event starts. At 8 h into the simulation, stations report wind speeds reaching approximately 14–20 m/s (31–45 mph or 50–72 km/h). The model captured this initial stage fairly well. The Valley Center (VLCC1) station (Fig. 5c) shows a slight delay in the arrival of the Santa Ana event, but after a couple of hours of simulation the WRF forecasted wind speed starts matching the observations. It is possible that the wind measurements at this particular station were affected either by the topography smoothed out at the model boundary or by the simulated too slow westward propagation of the Santa Ana event. The fact that the arrival of Santa Ana winds at the central stations (GOSC1 and KRNM) was captured correctly suggests that the former hypothesis is more probable.

The Witch Fire was ignited in the Witch Creek area east of Ramona, California, almost exactly 8 h into the simulation when the wind speed picked up. A violent easterly wind caused electrical power-line arching that ignited the fire (Maranghides and Mell, 2011). At that time the Pine Hill station (PIHC1; Fig. 2) reported wind speeds of 20 m/s (45 mph or 72 km/h). Fig. 5a shows that simulated wind speeds near the ignition location are also close to 20 m/s. Note that even though the local wind speed is captured very well at time of ignition, the model has some problems capturing local wind directions. As shown in Fig. 5a, the forecasted wind direction is almost steady and easterly, while the Pine Hill (PIHC1) station reported variable wind directions. The wind had a northerly component at PIHC1, while the three other stations reported mainly easterly winds with only a slight northerly component. This problem is also evident in the statistics presented in Tables 2 and 3, showing for this station relatively good agreement with observations in terms of the wind speed but poor in terms of the wind direction.

The Guejito Creek Fire (also called the Guejito Fire) started 12 and a half hours later at 1:00 am Monday, October 22, 2007 at the Guejito Creek drainage, on the South Side of California State Route 78 and 0.4 km (1/4 mile) west of Bandy Canyon Rd., or 10 km (6 miles) northeast of The Trails. The cause of ignition was identified as energized power lines contacting a lashing wire (Maranghides and Mell, 2011).

After a slight decrease in the wind speed at roughly 12 h into the simulation, the Santa Ana winds strengthened again, reaching almost 25 m/s (56 mph or 90 km/h) 12 h later. Fig. 5 shows that the model captures this drop and increase in the wind speed relatively well, but this varies among the analyzed locations. At the Goose Valley (GOSC1) station (Fig. 5b), the model forecasts the wind directions better than at other locations, but significantly overestimates the observed wind speed (see Tables 3 and 2, respectively). Fortunately the fire front was still a ways east at the time, where the wind speed forecast is significantly better (see Fig. 5a). It is therefore likely that this discrepancy between the wind forecasts and observations did not significantly impair the fire spread forecast for this time period.

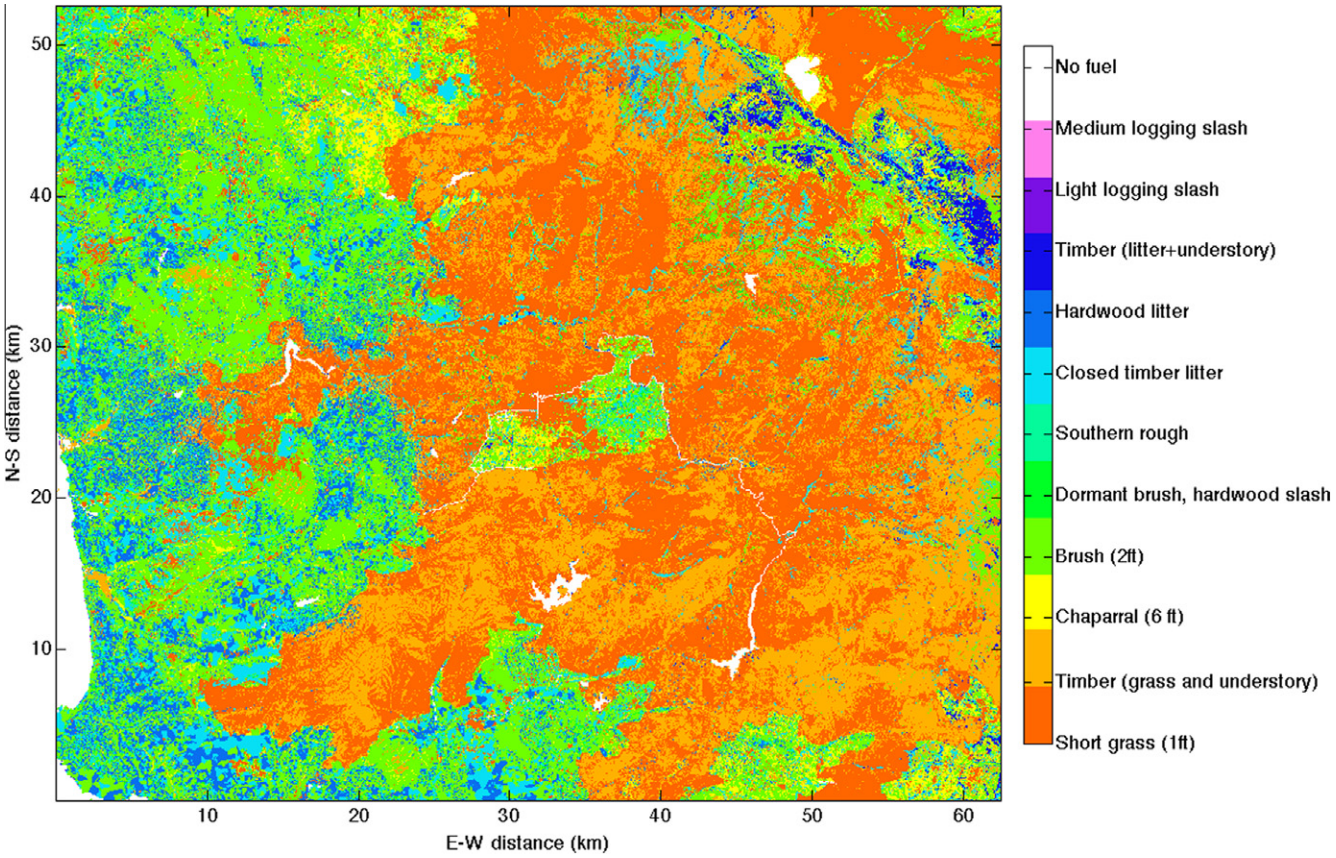

Fig. 3. Fuel map used in the WRF–Sfire simulation according to the 13 Albini (1976) fuel categories.

During the next 24 h (up to 48 h into the simulation) the wind speed gradually decreased (Fig. 5). The model generally captured this trend. There are however some discrepancies. A comparison between observations and model results at Pine Hill, the eastern-most station in the fire domain, shows that after 36 h into the simulation there is a positive bias in the model results (Table 2; PIHC1; ME of 2.9 m/s). For Goose Valley (Fig. 5b) the modeled wind speed is overestimated as well, but not consistently as in the case of the Pine Hill station. The Goose Valley station reported significantly higher wind speed variability compared to the other three stations. This station is located in a narrow (roughly 1 km) valley surrounded by the mountains from the west, east and south. Therefore, it is possible that the small-scale flow features, including down slope and canyon winds induced by the complex topography of this region, were not modeled well, and led to discrepancies between the simulated and observed wind speed.

For the Valley Center (Fig. 5c) the forecasted wind speed and direction remain in good agreement with observations for the most of the simulated period. However, between 36 and 48 h into the simulation there is a period of noticeable bias in the forecasted wind direction, which resulted in a significant increase in the directional error: 11.2° for the first 36 h versus 15.3° for the whole simulation. Also during this period, the forecasted wind speed stayed between 17 and 18 m/s, while the VLCC1 station recorded a drop from 18 m/s to 12 m/s, followed by a rise back to 18 m/s. This decrease in the wind speed was associated with a change in the wind direction from east–north–east to east–south–east, which was completely missed by the model. This station is located just 2.8 km (five grid points) south from the northern domain boundary, in a region directly affected by the outer domain (D03). This distance is too short to allow the inner domain to resolve a local flow. The first five grid points (relaxation zone) are used to blend the outer domain forcing into the inner domain. Therefore, at that distance from the boundary the forcing coming from the outer domain may dominate, deteriorating the results near the border of the inner one.

Due to the technical problems of the Ramona Airport station (KRNM), the model results between 32 h and 50 h cannot be validated for this location. Nonetheless, during the period of the first 30 h for which data are available, the simulated wind speed and direction tend to follow the observations, but without the observed variability. As a consequence, for this station, the mean errors are small but correlation coefficients are low (see Tables 1 and 2).

A reliable numerical weather forecast for a 72 h period is a challenge for any weather forecasting model. The analysis of the wind speed forecast indicates that the predictability drops significantly after 36 h. The statistics computed for the first 36 h of the simulation compared to the whole 72 h show this clearly. The model error accumulates in time to a degree that it spoils the results. The operational solution is to run the model daily as current upper air and surface data are available, rather than continue one 72 h run from a "cold start".

4.2. Fire spread forecast

Due to limited availability of fire progression data, the validation of the simulated wildfire spread can be more difficult than the validation of a meteorological forecast. Meteorological data are normally available from automated weather stations at 1 h intervals at least. Fire data often contain only the final fire perimeter that is, in most cases, the product of post-fire analysis. In this study we were fortunate enough to obtain twice-daily progression maps prepared by the California Emergency Management Agency.

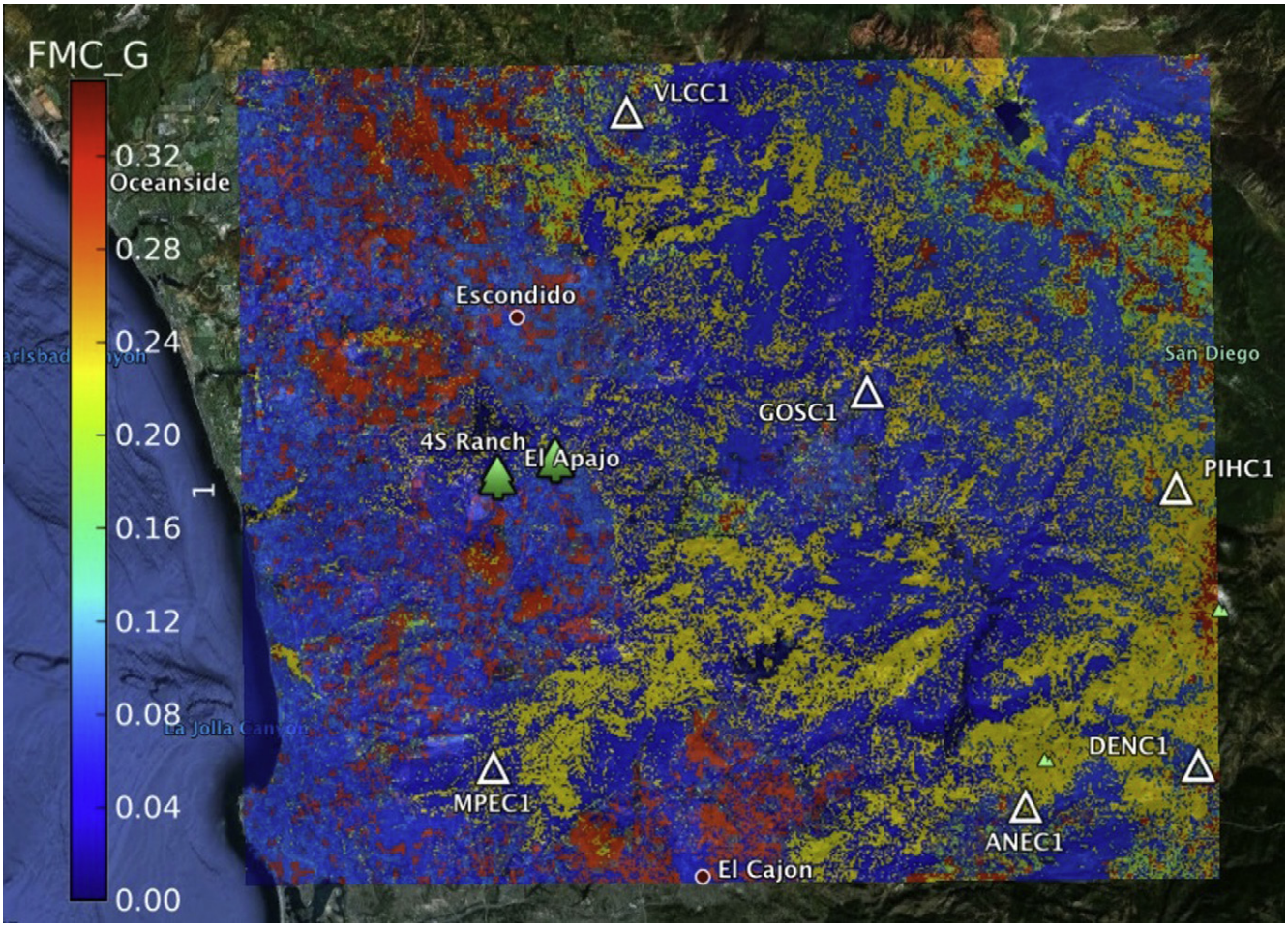

Fig. 4. Fuel moisture map used during the simulation as well as the locations of surface stations used for estimating 10 h fuel moisture (white triangles) and live fuel moisture (green tree icons). (For interpretation of the references to color in this figure legend, the reader is referred to the web version of this article.)

Table 2
Statistical analysis of the wind speed forecast.

Statistical measure/station	PIHC1	GOSC1	VLCC1	KRNM
Statistics for the first 36 h of the simulation				
ME (m/s)	2.9	3.9	−0.6	−0.6
MAE (m/s)	3.1	4.6	2.2	3.6
RMS (m/s)	3.6	5.1	2.9	4.9
R	0.85	0.76	0.87	0.26
Statistics for the whole simulation period (1–72 h)				
ME (m/s)	3.3	5.9	0.0	-0.6
MAE (m/s)	3.4	6.4	3.1	3.7
RMS (m/s)	3.8	7.5	4.0	4.9
R	0.87	0.59	0.69	0.29

Table 3
Statistical analysis of the wind direction forecast.

Statistical measure/station	PIHC1	GOSC1	VLCC1	KRNM
Statistics for the first 36 h of the simulation				
ME_C (deg)	7.9	−5.5	−1.2	−3.4
MAE_C (deg)	21.0	8.7	11.2	14.6
RMS_C (deg)	27.0	12.0	14.9	18.5
Mean observed WD (deg)	73.1	73.3	74.6	73.6
Mean simulated WD (deg)	81.6	67.6	74.5	70.1
R_C	−0.031	0.150	−0.506	−0.150
R_T	0.035	0.144	−0.583	−0.155
Statistics for the whole simulation period (1–72 h)				
ME_C (deg)	6.5	−6.3	0.0	−2.6
MAE_C (deg)	17.8	12.0	15.3	14.8
RMS_C (deg)	24.3	15.6	20.9	19.7
Mean observed WD (deg)	71.0	75.0	74.4	74.7
Mean simulated WD (deg)	81.7	68.0	72.0	70.8
R_C	−0.039	0.112	−0.220	0.066
R_T	0.014	0.112	−0.184	0.097

This allowed us to not only look at the final burnt area, but also examine the fire perimeter during the fire progression.

4.2.1. Fire progression

To reconstruct the propagation of the Witch and Guejito fires, four fire perimeter maps available for the period of the simulation were used. Two show the later stage of the Guejito fire and the other two present the Witch fire before the two fires merged. Additionally, the reports prepared by the California Department of Forestry and Fire Protection (CalFire) for incidents 07-CA-MVU-10432 (Witch fire) and CA-MVU-10484 (Guejito fire) were analyzed. These reports (available from http://www.fire.ca.gov/fire_protection/downloads/redsheet/) provide estimates of time and location of ignitions. Witness testimonies contained in these reports help to estimate the progression of the Witch and Guejito fires. Based on these testimonies, two distinct locations where the fires were observed were selected: Guejito bridge on HWY 78 at the origin of the Guejito fire; and the N-W boundary of Rancho Bernardo. These locations are marked, respectively, as a red circle and yellow square in Fig. 6. The reported timings of fire arrival at these locations were also used for the validation of the simulated fire spread.

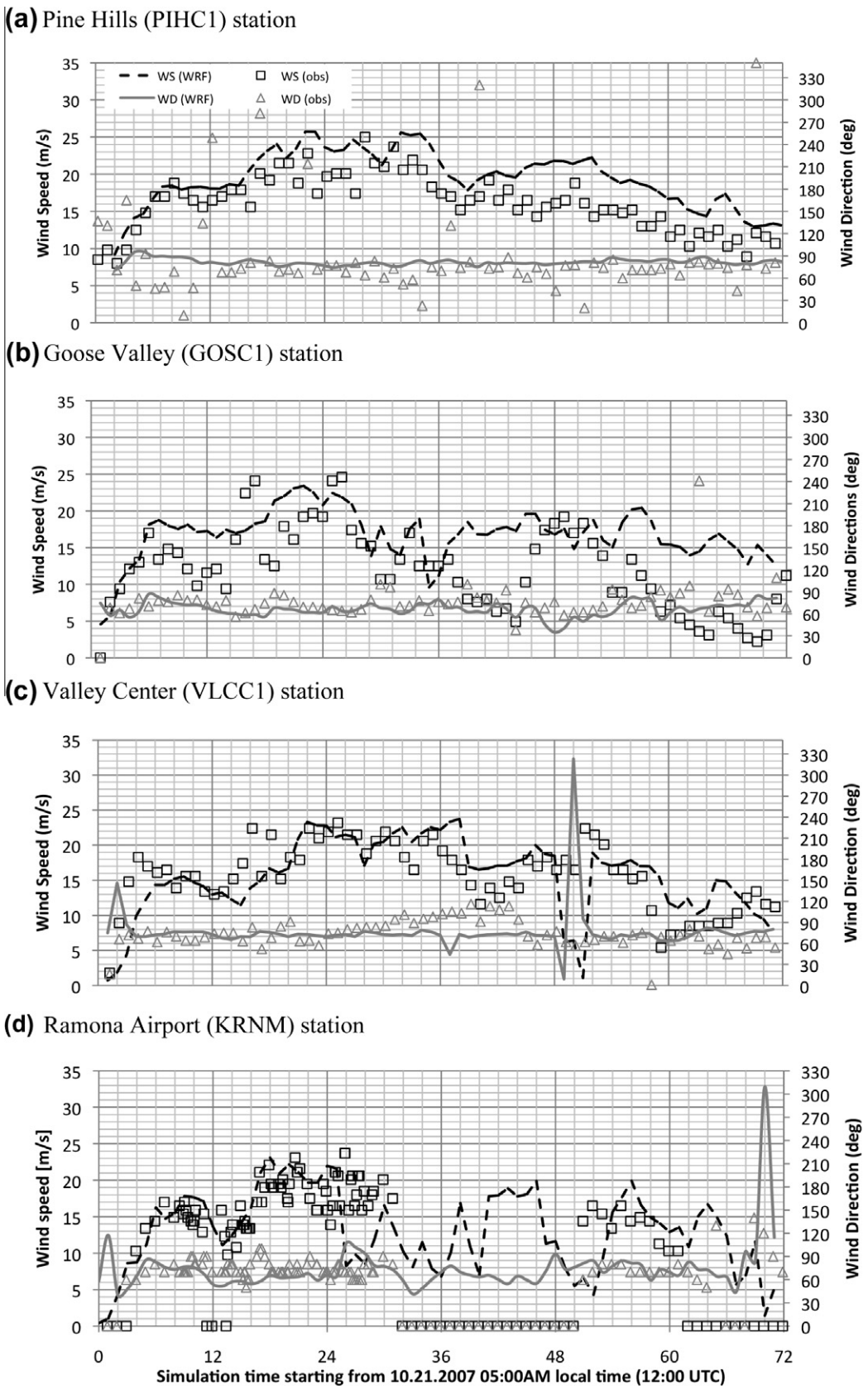

Fig. 5. Time series of WRF-simulated and observed wind speed (WS) and wind direction (WD).

The Witch fire was ignited about 3 km south-west from Santa Ysabel (see Fig. 8), and, driven by strong, easterly 20 m/s Santa Ana winds, propagated very quickly towards the south-west. Fig. 6a shows the Witch fire front advancing by almost 17 km,

reaching a ROS of 0.79 m/s (2.8 km/h) during the first 6 h. During the next 6 h, it expanded in the N–S direction, surrounded residential areas of Ramona, and extended rapidly toward Eagle Crest/Highland Road, position marked as an orange triangle in Fig. 6b.

The Geujito fire ignited at 1:00 am local time (20 h from the start of the simulation) and started its quick westward propagation; in the first 1 h and 45 min it advanced westward by more than 4 km. In Fig. 6b, the first estimate of the Guejito fire area (white contour) is overlaid with the model output (red contour) at 2:45 am local time. The initial growth of this fire is captured well and is confined within the fire perimeter contour estimated from observations. The next Guejito fire perimeter estimate was for 5:00 am local time. The comparison between the simulated and observed fire perimeters at that time also shows good agreement in terms of the size of the fire and direction of propagation (see Fig. 6c). Where and when the Witch and Guejito fires merged were also well captured. In the simulation, the fires merged at the Guejito bridge at 8:00 am, while the reported time of Witch arrival at this location was just 15 min earlier (see Fig. 6d). One of the witnesses whose property was destroyed reported that Guejito burnt the north-eastern part of his land, and a couple of hours later the Witch fire advancing from the south-east burnt the rest. Simulated fire behavior is consistent with this testimony. Fig. 6c and d indicates that the area south from the Guejito creek could have been affected initially by the Guejito fire and then by the Witch fire approaching from the S-E.

After merging, both fires continued to advance toward Rancho Bernardo, increasing their N–S extent (see Fig. 6e). The Santa Ana system advanced from the east, gradually weakening as it approached the coast. Therefore the wind speed over the western part of the fire domain was significantly lower than it was in the center and eastern parts. This change in wind strength, together with higher fuel moisture in the western part of the domain, may explain the significant fire deceleration evident in Fig. 6d and e.

Records of firefighters' interventions in Rancho Bernardo suggest that the fire reached its N-W boundary around 11:30–12:30 local time, roughly 6 h after burning properties on its N-E edge. According to the WRF–Sfire forecast, the fire reached the eastern side of Rancho Bernardo at 7:30 am, roughly 1 h later than observed, then went around it and reached its western side roughly 1 h earlier than observed. Fig. 6c shows the simulated fire perimeter extending past Rancho Bernardo at 11:30 am. Fig. 6f shows the observed and simulated fire perimeters at the time when the Witch fire perimeter was first estimated. Fig. 6c indicates that 15 h after the previous fire area estimate, the modeled fire area still matches the observational estimates. The southern extent of the eastern fire flank is slightly overestimated, but the general shape and size are captured well. Fig. 6g and h shows further fire progression. The E–W extent of the fire did not increase significantly after 8 pm (Fig. 6f), but its N–S spread continued. The fire, after consuming most of the fast-burning grassy fuels types (yellow and orange colors[1] on fuel map shown in Fig. 3), reached an area with less combustible fuel types and slowed down. Compared to an early WRF–Sfire simulation using a constant fuel moisture content of 6.5% (not shown), the spatially-varying initial fuel moisture produced a significantly improved fire perimeter forecast. Fig. 6h shows the simulated fire area overlaid with the observed perimeter on October 23 at 15:00. Except for the fire flank spreading N-W around Escondido where the simulated fire extends much further than the observed, the simulated fire matches observations in both shape and size.

[1] For interpretation of color in Fig. 3, the reader is referred to the web version of this article.

4.2.2. Burnt area and fire perimeter

There is no definite point when a WRF–Sfire simulated fire stops. The model fire continues to burn as long as there is combustible material in its way. Since the model does not account for any fire suppression actions taken during the fire, for the sake of comparison with the observed final fire perimeter, the time when the model fire reaches its relatively steady perimeter may be considered as the final fire perimeter. Fig. 7 shows the total burnt area and change in equivalent fire diameter at 10 min intervals for the simulation. This plot is used to identify the period of time when the WRF simulated area matches the observed one and the model fire "stops" propagating.

The final fire area reported by CalFire was estimated to be 80,156 ha. As shown in Fig. 7, the simulated fire area reached this value roughly 60 h into the simulation (24.10.2007 00:00 UTC). This moment is used for validation of the WRF–Sfire simulated fire area presented in Fig. 8.

The fire areas from previous estimates shown in Fig. 6f and g are added in Fig. 7 as square points. It has to be mentioned that the fire area estimates performed during the fire had some error. The analysis of the fire progression maps showed that in some cases the earlier fire area estimates contain regions that were not classified as burnt areas even in the final post-fire perimeter estimate. We treated the ratio of the erroneously classified area to the total area at any given time as the error interval in the fire area estimate and plotted it on Fig. 7. Note that the initial fire estimates tend to be crude with large error bars, and then more precise with smaller error bars as more data become available.

Additionally, Fig. 7 shows changes in time in the equivalent fire diameter, computed as the diameter of a circle having the same area as the simulated. This is used as a measure of the rate of fire perimeter growth. Fig. 7 shows that the relative changes in the equivalent fire perimeters are very low for the time when the simulated fire area matched the observed one (i.e., 0.49% at 60 h into the simulation). This suggests that, even though the simulated fire did not stop completely, a near-zero change in the relative diameter could be used to define the end of its active spread.

Fig. 8 shows that even though the simulated fire area is generally overestimated, the general shape of the fire perimeter is captured well. Also, the overall N–S and E–W extent of the simulated fire is pretty close to observations. However, there are also some regions of discrepancies between simulated and observed fire perimeters that are marked in Fig. 8 using color ovals. The simulated fire did not reach as far north (see yellow ovals in Fig. 8) as the observed final fire perimeter suggests. The elevation between the northern edge of the simulated fire and the northern edge of the observed final perimeter changes by roughly 350 m over a distance of 7 km. This inclination (below 3°) is not large enough to generate any measurable upslope ROS. This suggests that it was a southerly wind component that drove the fire perimeter north. The wind speed measured at the VLCC1 station (see Fig. 5c) indicates that there was a period of southeasterly wind (wind direction around 110°) between 36 and 48 h, but the model did not capture this shift in the wind direction. Fig. 5c shows that during this period the model predicted a wind direction of 80° and higher wind speeds than observed. There is no guarantee that the wind speed conditions recorded by the VLCC1 station can be treated as representative for the disagreement area we consider. Nonetheless, if the measured southerly wind component of 4.4 m/s was supplied to the Rothermel model, the WRF–Sfire fire could have advanced quickly over the grassy fuel by about 8 km in that time, which is over twice the width of the gap between the observed and simulated fire perimeter.

Another region where the simulated fire perimeter does not match the observed final perimeter is along the south-eastern edge of the fire marked by the orange oval in Fig. 8. The wind speed and

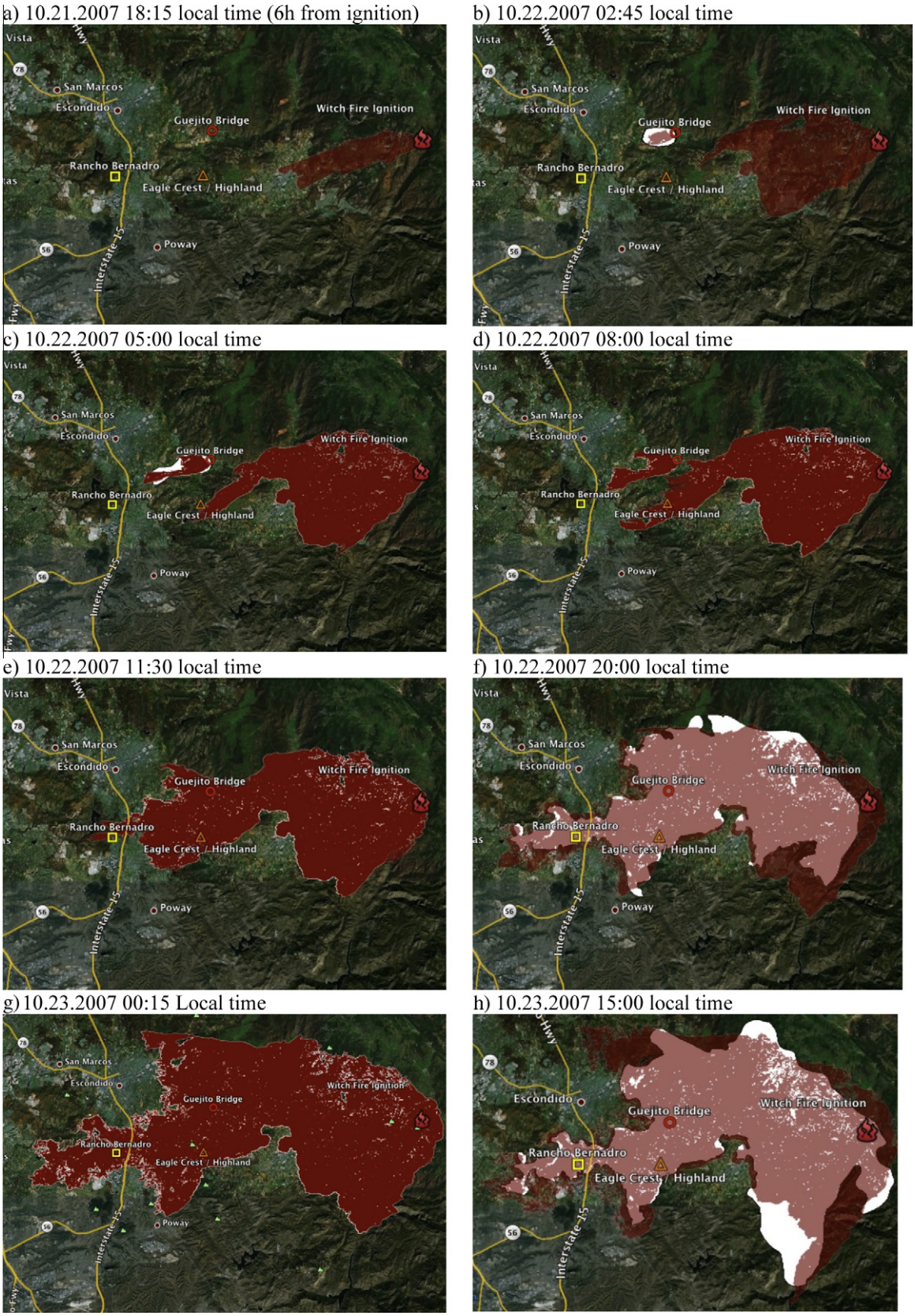

Fig. 6. Simulated (red) and observed (white) areas of the Witch and Guejito fires. Image overlay prepared using Google Earth. (For interpretation of the references to color in this figure legend, the reader is referred to the web version of this article.)

direction time series from the nearby PIHC1 station (Fig. 5a) also shows slight discrepancies between the simulated and measured wind directions that potentially could have contributed to this mismatch. During the first 12 h into the simulation, during the per-

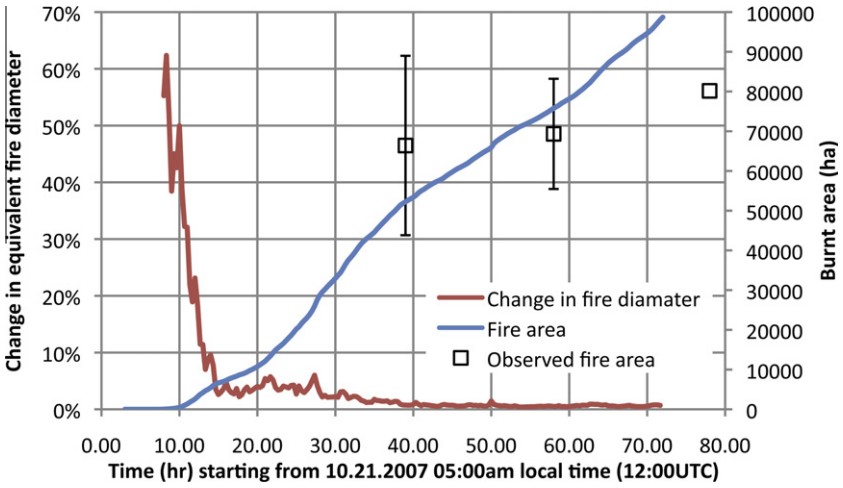

Fig. 7. Time series of the simulated burnt area (blue line), and the relative change in the equivalent fire diameter (red line), together the fire area derived from perimeters estimated by the California Emergency Management Agency, and the final perimeter estimated by CalFire (last point without error bars). (For interpretation of the references to color in this figure legend, the reader is referred to the web version of this article.)

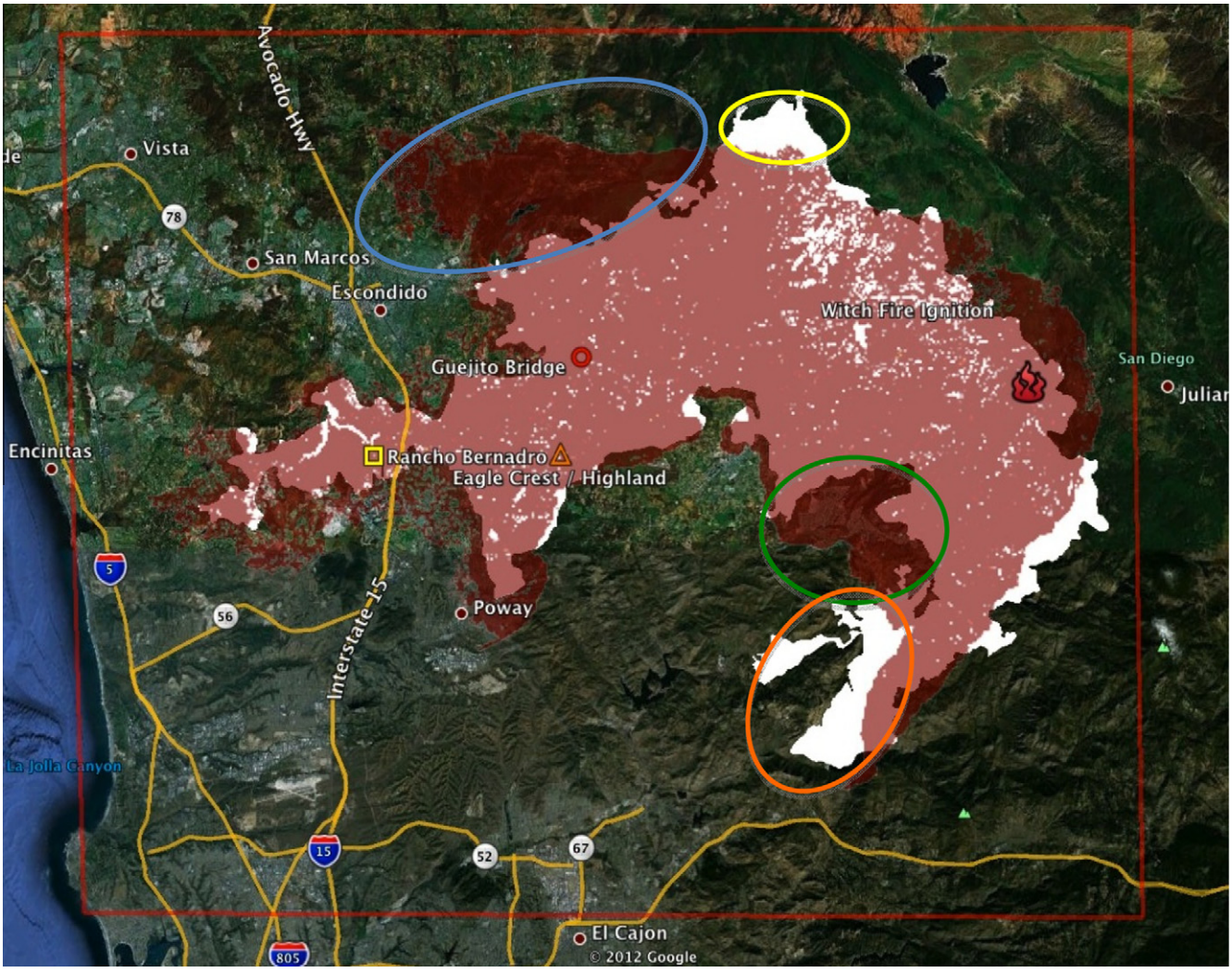

Fig. 8. Observed final perimeter (white) versus WRF–Sfire simulated fire area (red) on 23.10.2007 17:00 local time (60 h into simulation). (For interpretation of the references to color in this figure legend, the reader is referred to the web version of this article.)

iod of increasing wind speed, there were a few reports of winds with a northerly component. However, since these shifts in the wind direction were only temporary, they cannot be treated as the only reason for the observed discrepancies. Close examination of the fuel map suggests that the El Capitan reservoir and the San Diego River blocked the fire progression in the model simulation.

As a consequence the modeled fire stopped at the eastern shore of these water bodies and did not extend westward as observed.

The blue and green ovals in Fig. 8 highlight regions that were burnt in the WRF–Sfire simulation but not in reality. The blue oval shows the residential area north of Escondido and the green one corresponds to San Diego Estates. In the first case it is hard to speculate what could be the reason. The fact that we did not observe this problem in the initial simulation with a constant, relatively high, moisture content of 6.5%, suggests that we might have underestimated the fuel moisture in this region. However, this problem may be also associated with the general trend of the Rothermel model to overestimate the fire spread rate in grass fuels (Mell et al., 2007). On another hand, during Santa Ana events the wind speed affects the chaparral fire spread three times stronger than any other parameter (Clark et al., 2008), which suggests, that the local overestimation of the simulated wind speed could also be a reason for the over predicted fire extent N-W from Escondido. In the case of the region marked by the green oval, representing San Diego Estates, a possible reason for the observed discrepancies is the fuel misclassification. This residential area was not marked as incombustible, so the model fire advanced through it.

The Guejito and Witch fires burned for 10 days. During this period various suppression actions were taken that probably affected the fire shape, but that are not purposely accounted for in the simulation. Also, the simulation ends much earlier (roughly 65 h after Witch fire ignition) than the time the final fire perimeter was reconstructed from post-fire operations. However, the daily fire perimeter estimates used in this study seem to confirm that the fire progression during the Santa Ana winds was captured realistically in terms of perimeter shape and observed fire arrival times at selected check points.

5. Summary and conclusions

This pilot study demonstrates that it is possible to use WRF–Sfire, a fluid-dynamical deterministic modeling system, to provide a numerical forecast of wildfire behavior and spread in a landscape setting in real-time. The entire 72 h forecast analyzed in this study was computed within 4 h 48 min, while the first 24 h forecast was available in just 1 h 35 min. This computational performance proves that it is feasible to use the coupled WRF–Sfire atmosphere–fire simulation for real-time wildfire forecasting.

As discussed in the Introduction, the primary physical advantage of the WRF–Sfire is that the WRF–Sfire's fluid-dynamical approach to wildfire forecasting includes the ability to model wind and coupled atmosphere/wildfire interactions. The spatially-gridded GIS data on fuels and topography, along with meteorological data from the national network of weather observations, can be easily ingested using the operational WRF pre-processing system (WPS). The WPS allows for feeding the model 'future' boundary conditions extracted from larger-scale operational numerical forecasts. These features make the WRF–Sfire a weather- and fire-forecasting model suitable for real world simulations. Although not done in the Santa Ana WRF–Sfire simulation in this study, meteorological data from the national network of weather observations collected after the model start can be used by the operational WRF-DA (Data Assimilation system) to update and improve a WRF–Sfire forecast. Once a WRF weather forecast at the relatively coarse (operational) resolution is made, the system's nested-grid capabilities can provide a real-time forecast of velocity, temperature, and moisture fields at the fine resolution of the fire domain.

Simulation of wind, temperature, and moisture in the fire domain is sensitive to the lateral boundary conditions at its horizontal border. If these boundary conditions are not accurate, the simulated fields in the fire domain deteriorate. There is also a margin within each nested domain that is used to blend the lower resolution data from the outer domain into the higher resolution of the inner (nested) domain. Within and close to this zone the results should be treated with some skepticism since they are strongly affected by the coarser outer domain that is not capable of resolving fine features expected to be seen in the finer, nested domain. We suspect that this could be a reason for some of the discrepancies between the simulated and observed winds at the VLCC1 station, located just at the northern border of the fire domain.

As shown in Section 4.1, WRF prediction of high wind speeds was done well, while prediction of weak winds, especially at lower elevations and in mountain valleys, was not. Comparisons to available observations indicate that the magnitudes of WRF forecasted weak and gusty low-elevation winds and down-slope or lee-slope winds were generally overestimated. Even though the average wind direction was simulated well, there were some intermittent discrepancies between simulated and observed wind speeds, especially at PIHC1, the most northern meteorological station in the fire domain, and to smaller degree, at VLCC1, the most eastern station (see periods 12–24 h and 36–48 h into simulation in Fig. 5a and c). The overall mean error between the simulated and observed wind direction was rather small (between -2.6° and 6.5°). However WRF did not mange to capture observed hourly variations in the wind direction, with the result that there is practically no correlation between the simulated and observed wind direction (see Table 3).

The accuracy of the WRF–Sfire for operational use was judged based on a comparison between observed and forecasted fire progression as well as observed and simulated final fire perimeters. The agreement overall between the observed and simulated fire perimeters was good. Wherever the model overestimated the burnt area was attributed, at least partially, to the generally overestimated wind speed. The problems with realistic rendering of hourly variations in the wind direction could also impair the fire spread forecast. Nonetheless, the fire spread data for the center part of domain confirm that the most active progression of the fire perimeter during the Santa Ana winds was captured well, with a mismatch between the simulated and observed timing of the fire arrival of 1 h or less.

It is noted that the modeled fire perimeter is very sensitive to the wind forecast. When the Rothermel formula moves the fire a certain distance ahead based on the WRF–Sfire winds, it can never move the fire back to the previous location. In other words, forecast errors in simulated ROS accumulate in time. Therefore even a relatively accurate wind forecast may be not good enough to provide an equally accurate fire perimeter forecast.

Another source of error may be the static fuel moisture used in the study. As reported by Jolly (2007), the Rothermel spread-rate formula is very sensitive to changes in fuel moisture content that are hard to estimate precisely. Introduction of the spatially-varying fuel moisture into the WRF–Sfire at ignition significantly improved the subsequent fire spread prediction, as compared to previous simulations performed with a spatially uniform (set to a constant 6.5%) fuel moisture content. The results suggest that adding a spatially- and temporally-varying fuel moisture model to WRF–Sfire, along with better techniques for assimilation of the initial fuel moisture data, would further improve the model results. The humidity measurements show an increase in the relative humidity during the second half of the simulation. A temporally-varying moisture model could have captured the corresponding rise in the fuel moisture, and reduced the final fire area, which was overestimated.

Another source of error in the simulation of the Santa Ana fires may be the impact of sloping terrain on fire spread. The Rothermel formula used in WRF–Sfire has a slope correction factor that provides upslope fire spread in the wind direction normal to the local fire perimeter when the slope incline is greater than zero. At the

same time, the WRF–Sfire wind was modified by terrain, especially steep terrain. In many circumstances, steep terrain is a source of energy for the wind that accelerates upslope flows (Markowski and Richardson, 2010). In the simulation of the Santa Ana fires, the fire perimeters propagated mostly downwind and so likely did not experience "double-counting." However, in general, this may introduce error.

Despite the discrepancies between observed and simulated final fire spread, the results of the study indicate a potential for operational application of WRF–Sfire. However, before this model can become a fire-forecasting tool, its current limitations have to be addressed. The lack of mechanisms allowing for crown fire modeling in the current version limits the model applicability to surface fire only. Also, the current version of WRF Sfire does not model spotting, limiting its forecast capabilities when spotting does occur. The simulations performed for the sake of this study indicated great model sensitivity to the fuel moisture used as an input. One way to improve model capabilities would be to implement a fuel moisture model coupled directly with the current atmospheric core.

More accurate or confident prediction of fire behavior and propagation prediction by WRF–Sfire would have many possible uses for the wildfire management community. These can include: wildland fire evacuation planning; effective and safe deployment of aerial and ground resources; predicting wildfire and prescribed fire intensity/severity that may vary under changing local meteorological and terrain conditions; where and how to fight wildfire, for example, to prevent wildland–urban interface fires or when attempting to control wildfire in ecosystems that need protection from smoke or are at risk of severe fire damage.

Acknowledgments

This research was supported in part by National Institute of Standards and Technology (NIST), Fire Research Grants Program, Grant 60NANB10D225 and in part by a grant from the Natural Sciences and Engineering Research Council of Canada. A gratis grant of computer time from the Center for High Performance Computing, University of Utah, is gratefully acknowledged. This research was partially supported by NSF grants ATM-0835579 and DMS-1216481. This work partially utilized the Janus supercomputer, supported by the NSF grant CNS-0821794, the University of Colorado Boulder, University of Colorado Denver, and National Center for Atmospheric Research.

We would also like to thank Ms Kris Higgs from California Emergency Management Agency for help with obtaining the fire perimeter data, as well the anonymous reviewers who provided us with very valuable comments.

References

Albini, F., 1976. Estimating Wildfire Behavior and Effects. Technical Report Report INT-30. USDA Forest Service, Intermountain Forest and Range Experiment Station, Ogden, UT.

Andrews, P., 1986. Behave: Fire Behavior Prediction and Fuel Modeling System – Burn Subsystem. Part 1. Technical Report General Technical Report INT-194. USDA Forest Service, Intermountain Forest and Range Experiment Station, Ogden, UT, 130 pp.

Beezley, J.D., Kochanski, A., Kondratenko, V.Y., Mandel, J., Sousedik, B., 2010. Simulation of the Meadow Creek Fire Using WRF-Fire, Poster at AGU Fall Meeting 2010. <http://www.openwfm.org/wiki/File:Agu10jb.pdf>.

Beezley, J.D., 2011. Importing High-Resolution Datasets into Geogrid. Paper P2, 12th WRF Users' Workshop. National Center for Atmospheric Research, June 20–24, 2011.

Beezley, J.D., Kochanski, A.K., Kondratenko V.Y., Mandel J., 2011. Integrating High-Resolution Static Data into WRF for Real Fire Simulations. Paper 6.3, Ninth Symposium on Fire and Forest Meteorology, Palm, Springs, October 2011.

Bossert, J.E., Linn, R.R., Reisner, J.M., Winterkamp, J.L., Dennison, P., Roberts, D., 2000. Coupled Atmosphere–Fire Behavior Model Sensitivity to Spatial Fuels Characterization. Third Symposium on Fire and Forest Meteorology of the American Meteorological Society, January 9–14, 2000, Long Beach, CA, pp. 21–26.

Clark, T., Coen, J., Latham, D., 2004. Description of a coupled atmosphere–fire model. International Journal of Wildland Fire 13 (1), 49–63.

Clark, R.E., Hope, A.S., Tarantola, S., Gatelli, D., Dennison, P.E., Moritz, M.A., 2008. Sensitivity analysis of a fire spread model in a chaparral landscape. Fire Ecology 4 (1), 1–13.

Coen, J.L., 2005. Simulation of the big Elk fire using coupled atmosphere–fire modeling. Journal of Wildland Fire 14, 49–59.

Colman, Jonah J., Linn, R.R., 2007. Separating combustion from pyrolysis in HIGRAD/FIRETEC. International Journal of Wildland Fire 16 (4), 493–502, http://dx.doi.org/10.1071/WF06074.

Dobrinkova, N., Jordanov, G., Mandel, J., 2011. WRF-fire applied in Bulgaria. In: Dimov, I., Dimova, S., Kolkovska, N. (Eds.), Numerical Methods and Applications. Lecture Notes in Computer Science, vol. 6046. Springer, Berlin/Heidelberg, pp. 133–140. http://dx.doi.org/10.1007/978-3-642-18466-615

Fisher, N.I., Lee, A.J., 1983. A correlation coefficient for circular data. Biometrika 70 (2), 327–332. http://dx.doi.org/10.1093/biomet/70.2.327.

Fosberg, Michael A., O'Dell, Clyde A., Schroeder, Mark J., 1966. Some characteristics of the three-dimensional structure of Santa Ana winds. Berkeley, Calif., Pacific SW. Forest & Range Exp. Sta. 35 pp., illus. (U.S. Forest Serv. Res. Paper PSW-30). <http://www.fs.fed.us/psw/publications/documents/psw_rp030/psw_rp030.pdf>.

Jammalamadaka, S.R., Lund, U.J., 2006. The effect of wind direction on ozone levels: a case study. Environmental and Ecological Statistics 13 (3), 287–298, dx.doi.org/DOI 10.1007/s10651-004-0012-7.

Jammalamadaka, S.R., SenGupta, A., 2001. Topics in Circular Statistics. World Scientific, NJ.

Jolly, W.M., 2007. Sensitivity of a surface fire spread model and associated fire behaviour fuel models to changes in live fuel moisture. International Journal of Wildland Fire 16, 503–509.

Jordanov, G., Beezley, J.D., Dobrinkova, N., Kochanski, A.K., Mandel, J., Sousedík, B., 2011. *Simulation of the 2009 Harmanli fire (Bulgaria)*, 8th International Conference on Large-Scale Scientific Computations, June 6–10, 2011, Sozopol, Bulgaria. Lecture Notes in Computer Science, Springer, to appear. arXiv:1106.4736

Keeley, J.E., Safford, H., Fotheringham, C.J., Franklin, J., Moritz, M., 2009. The 2007 southern California wildfires – lessons in complexity. Journal of Forestry 107, 287–296.

Kochanski, A., Jenkins, M., Krueger, S. K., Mandel, J., Beezley, J. D., Clements, C.B., 2010. Evaluation of The Fire Plume Dynamics Simulated by WRF-Fire. Presentation at AGU Fall Meeting 2010. <http://www.openwfm.org/wiki/File>.

Linn, R.R., Winterkamp, J.L., Weise, D.R., Edminster, C., 2010. A numerical study of slope and fuel structure effects on coupled wildfire behaviour. International Journal of Wildland Fire 19, 179–201.

Mandel, J., Beezley, J.D., Coen, J.L., Kim, M., 2009. Data assimilation for wildland fires: ensemble Kalman filters in coupled atmosphere–surface models. IEEE Control Systems Magazine 29, 47–65. http://dx.doi.org/10.1109/MCS.2009.932224.

Mandel, J., Beezley, J.D., Kochanski, A.K., 2011. Coupled atmosphere–wildland fire modeling with WRF 3.3 and SFIRE 2011. Geoscientific Model Development 4, 591–610.

Maranghides, A., Mell, W., 2011. A case study of a community affected by the Witch and Guejito wildland fires. Fire Technology 47 (2), 379–420.

Markowski, P., Richardson, Y., 2010. Mesoscale Meteorology in Midlatitudes, first ed. Wiley-Blackwell.

Mell, W., Jenkins, M.A., Gould, J., Cheney, P., 2007. A physics based approach to modeling grassland fires. International Journal of Wildland Fire 16, 1–22.

Papadopoulos, G.D., Pavlidou, F.-N., 2011. A comparative review of wildfire simulators. Systems Journal, IEEE 5 (2), 233–243. http://dx.doi.org/10.1109/JSYST.2011.2125230.

Patton, E.G., Coen, J.L., 2004. WRF-Fire: A Coupled Atmosphere–Fire Module for WRF. Preprints of Joint MM5/Weather Research and Forecasting Model Users' Workshop, Boulder, CO, June 22–25, NCAR, pp. 221–223.

Peace, Mika, Mattner, T., Mills, G., 2011. The Kangaroo Island bushfires of 2007. A meteorological case study and WRF-fire simulation. In: Ninth Symposium on Fire and Forest Meteorology, Palm Springs, CA, October 18–20, 2011. <http://ams.confex.com/ams/9FIRE/webprogram/Paper192200.html>.

Rollins, M.G., 2009. LANDFIRE: a nationally consistent vegetation, wildland fire, and fuel assessment. International Journal of Wildland Fire 18, 235–249.

Rothermel, R.C., 1972. A Mathematical Model for Predicting Fire Spread in Wildland Fires. USDA Forest Service Research Paper INT-115.

Ryan, K.C., Lee, K.M., Rollins, M.G., Zhu, Z., Smith, J., Johnson, D., 2006. Landfire: National vegetation and fuel mapping for fire management planning. Forest Ecology and Management 234 (15), S220, http://dx.doi.org/10.1016/j.foreco.2006.08.247, ISSN 0378-1127. <http://www.sciencedirect.com/science/article/pii/S0378112706007870>.

Schroeder, M.J., 1964. Synoptic Weather Types Associated with Critical Fire Weather. USDA Forest Service, Pacific Southwest Research Station, Berkeley, CA. 492 p. <http://www.dtic.mil/cgi-bin/GetTRDoc?AD=AD0449630>.

Sedepian, L., 1980. On the vertical extrapolation of mean wind power density. Journal of Applied Meteorology 19, 488–493.

Skamarock, W.C., Klemp, J.B., Dudhia, J., Gill, D.O., Barker, D.M., Duda, M.G., Huang, X.-Y., Wang, W., Powers, J.G., 2008. A Description of the Advanced Research WRF version 3. NCAR Technical Note 475.

Sullivan, A.L., 2009. Wildland surface fire spread modelling, 1990–2007: 1: Physical and quasi-physical models. International Journal of Wildland Fire 18, 349–368.

Sun, R., Krueger, S.K., Jenkins, M.A., Zulauf, M.A., Charney, J.J., 2009. The importance of fire–atmosphere coupling and boundary-layer turbulence to wildfire spread. International Journal of Wildland Fire 18, 50–60.

Van Wagner, C.E., Pickett, T.L., 1985. Equations and FORTRAN Program for the Canadian Forest Fire Weather Index System. Canadian Forestry Service, Forestry Technical Report 33.

Weise, D.R., Chen, S.C., Riggan, P.J., Fujioka, F.M., 2007. Using High-Resolution Weather Data to Predict Fire Spread Using the FARSITE Simulator – A Case study in California Chaparral. In: 7th Symposium on Fire and Forest Meteorology, Oct. 22–25, 2007, Bar Harbor, ME. <http://ams.confex.com/ams/pdfpapers/126873.pdf>.